Supporting Information: Machine-Learning Methods Enable Exhaustive Searches for Active Bimetallic Facets and Reveal Active Site Motifs for CO_2 Reduction

Zachary W. Ulissi,[†,†] Michael T. Tang,[‡,†] Jianping Xiao,[‡,†] Xinyan Liu,[‡,†] Daniel A. Torelli,[¶,§] Mohammadreza Karamad,[†] Kyle Cummins,[§] Christopher Hahn,[‡,†] Nathan S. Lewis,[¶,§] Thomas F. Jaramillo,[‡,†] Karen Chan,[*,‡,†] and Jens K. Nørskov[*,‡,†]

†*SUNCAT Center for Interface Science and Catalysis, Department of Chemical Engineering, Stanford University, Stanford, California 94305*

‡*SUNCAT Center for Interface Science and Catalysis, SLAC National Accelerator Laboratory, Menlo Park, California 94025*

¶ *Division of Chemistry and Chemical Engineering, California Institute of Technology, Pasadena, California 91125, United States*

§*Joint Center for Artificial Photosynthesis*

E-mail: chank@slac.stanford.edu; norskov@stanford.edu

Neural Network Training Scheme

The Atomistic Machine-learning Potential (AMP) package was used for the neural network potential throughout this work. The descriptor was the gaussian fingerprint module with

default (guessed) symmetry functions and parameters and a cutoff of 6.5Å. The tflow module for the neural network regression and prediction was used, which implemented a standard dense neural network on the Google Tensorflow platform, and is mathematically equivalent to the scheme described in literature.[S1] Due to the large number of configurations necessary to fit, a large network with two hidden layers, each with 100 nodes was used. At each iteration, all of the collected DFT single point calculations were collected into a single training set. The network was fit progressively:

1. Fitting with 1000 steps of the ADAM optimizer, 0.8 dropout on the connected layers, no regularization, no force training, step size 0.01.

2. Fitting with 10,000 steps of the ADAM optimizer, 0.8 dropout on the connected layers, L1 regularization of 0.1, no force training, step size 0.001.

3. Fitting with 60,000 steps of the ADAM optimizer, 0.8 on the connected layers, no L1 regularization, force training on with coefficient 0.01, step size 0.001.

Error estimates were provided by drawing a sample of predictions with the dropout still turned on, effectively approximating a Gaussian Process.[S2] All training was completed using the GPU-accelerated version of tensorflow for accelerated fitting. Relaxations using the trained calculators were completed in parallel using the CPU version of tensorflow since the prediction process was primarily spent computing fingerprints and their derivatives, not on the neural network portion of the code.

Electronic Structure Methods

All electronic structure calculations are carried out via the open-source package Quantum ESPRESSO.[S3] The exchange-correlation energies are approximated using the BEEF-vdW[S4] functional which uses the generalized gradient approximation and includes a non-local van

der Waals correction. All slab calculations are preformed using a plane-wave basis (plane-wave cutoff of 500 eV, density-wave cutoff of 5000 eV) and the Brillouin zone is sampled by a 6x6x1 Monkhorst-Pack k-point mesh.[S5] The lattice constants of the bulk Ni, NiGa, Ni_3Ga, and Ni_5Ga_3 crystals is calculated by minimizing the energy of the 1x1x1 bulk unit cells (k-point sampling 6x6x6), starting from initial structures from the Materials Project.[S6] No spin polarization is included in any of the calculations. The free energy correction for CO was assumed to be independent of site type and was based on previous studies,[S7] for a total of +0.483 eV including ZPE and vibrational contributions. The free energy was further corrected by -0.2 eV to account for solvation, and +0.17 eV for known DFT overbinding.[S8] Calculation details for the electrochemical barriers are presented in.[S7]

Angle-Resolved XPS

XP spectra were collected on an AXIS Ultra DLD instrument (Kratos Analytical) at a background pressure of 10^{-9} Torr. High-intensity excitation was provided by monochromatic Al Kα X-rays having an energy of 1486.6 eV with an instrumental resolution of 0.2 eV full width at half-maximum. Photoelectrons were collected at 0° from the surface normal at a retarding (pass) energy of 80 eV for the survey scans, whereas a pass energy of 20 eV was used for the high-resolution scans. For angle resolved measurements the collection angle was increased in 10-20° increments up to 75°, the lens mode was set to electrostatic, and the slot aperture was used at a pass energy of 20 eV. Spectra were first collected on Ni foil to demonstrate surface sensitivity. An increase in the ratio of oxidized Ni to metallic Ni signal was observed at larger collection angles. Spectra were then collected for Ni_5Ga_3 before and after electrolysis (Figures S2 and S1. Although a Ni richening of the surface was noticed after a 2 hr electrolysis at -1.5 V vs. Ag/AgCl, Ga remains present in a 3.5:1 Ni:Ga ratio throughout the surface of the electrode. The peak energies were calibrated against the binding energy, EB, of the adventitious C 1s peak. For quantitative analysis, the XPS

signals were fitted using CasaXPS software (CASA Ltd., Teignmouth, United Kingdom) to symmetric Voigt line shapes that were composed of Gaussian (70%) and Lorentzian (30%) functions that employed a Shirley background.

Electrochemical measurements were performed under the same conditions as previous reports.[S9] Briefly, long-term electrolyses were run in 0.1 M Na_2CO_3 acidified to pH 7 with 1 atm CO_2. An Ag/AgCl (3 M NaCl) reference was used.

Micokinetic Selectivity and Coverage

The microkinetic model[S7] included predictions for the surface coverages (Figure S3) and the final selectivity towards either H_2 or CH_4 (Figure S4).

References

(S1) Khorshidi, A.; Peterson, A. A. *Comp. Phys. Comm.* **2016**, *207*, 310–324.

(S2) Gal, Y.; Ghahramani, Z. Dropout as a Bayesian approximation: Representing model uncertainty in deep learning. International Conference on Machine Learning (ICML). 2016; pp 1050–1059.

(S3) Giannozzi, P.; Baroni, S.; Bonini, N.; Calandra, M.; Car, R.; Cavazzoni, C.; Ceresoli, D.; Chiarotti, G. L.; Cococcioni, M.; Dabo, I.; Corso, A. D.; de Gironcoli, S.; Fabris, S.; Fratesi, G.; Gebauer, R.; Gerstmann, U.; Gougoussis, C.; Kokalj, A.; Lazzeri, M.; Martin-Samos, L.; Marzari, N.; Mauri, F.; Mazzarello, R.; Paolini, S.; Pasquarello, A.; Paulatto, L.; Sbraccia, C.; Scandolo, S.; Sclauzero, G.; Seitsonen, A. P.; Smogunov, A.; Umari, P.; Wentzcovitch, R. M. *J. Phys.: Condens. Matter* **2009**, *21*, 395502.

(S4) Wellendorff, J.; Lundgaard, K. T.; Møgelhøj, A.; Petzold, V.; Landis, D. D.; Nørskov, J. K.; Bligaard, T.; Jacobsen, K. W. *Phys. Rev. B* **2012**, *85*, 253149.

(S5) Monkhorst, H. J.; Pack, J. D. *Phys. Rev. B* **1976**, *13*, 5188–5192.

(S6) Jain, A.; Ong, S. P.; Hautier, G.; Chen, W.; Richards, W. D.; Dacek, S.; Cholia, S.; Gunter, D.; Skinner, D.; Ceder, G.; Persson, K. A. *APL Mater.* **2013**, *1*, 011002.

(S7) Liu, X.; Xiao, J.; Peng, H.; Hong, X.; Chan, K.; Nørskov, J. K. *Nat. Commun.* **2017**, *8*, 15438.

(S8) Abild-Pedersen, F.; Andersson, M. *Surf. Sci.* **2007**, *601*, 1747–1753.

(S9) Torelli, D. A.; Francis, S. A.; Crompton, J. C.; Javier, A.; Thompson, J. R.; Brunschwig, B. S.; Soriaga, M. P.; Lewis, N. S. *ACS Catal.* **2016**, *6*, 2100–2104.

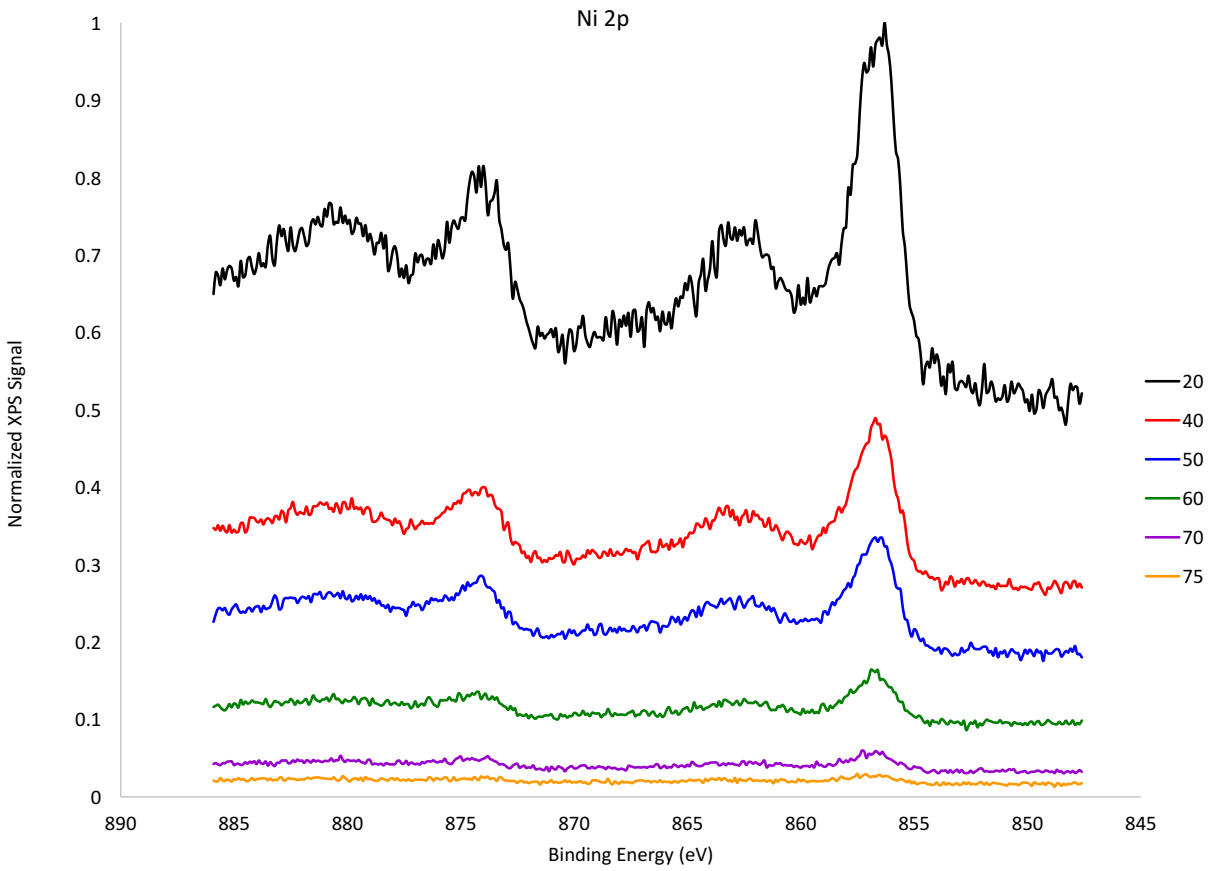

Figure S1: Nickel 2p angle resolved XPS (ARXPS) spectra, after electroduction as described.

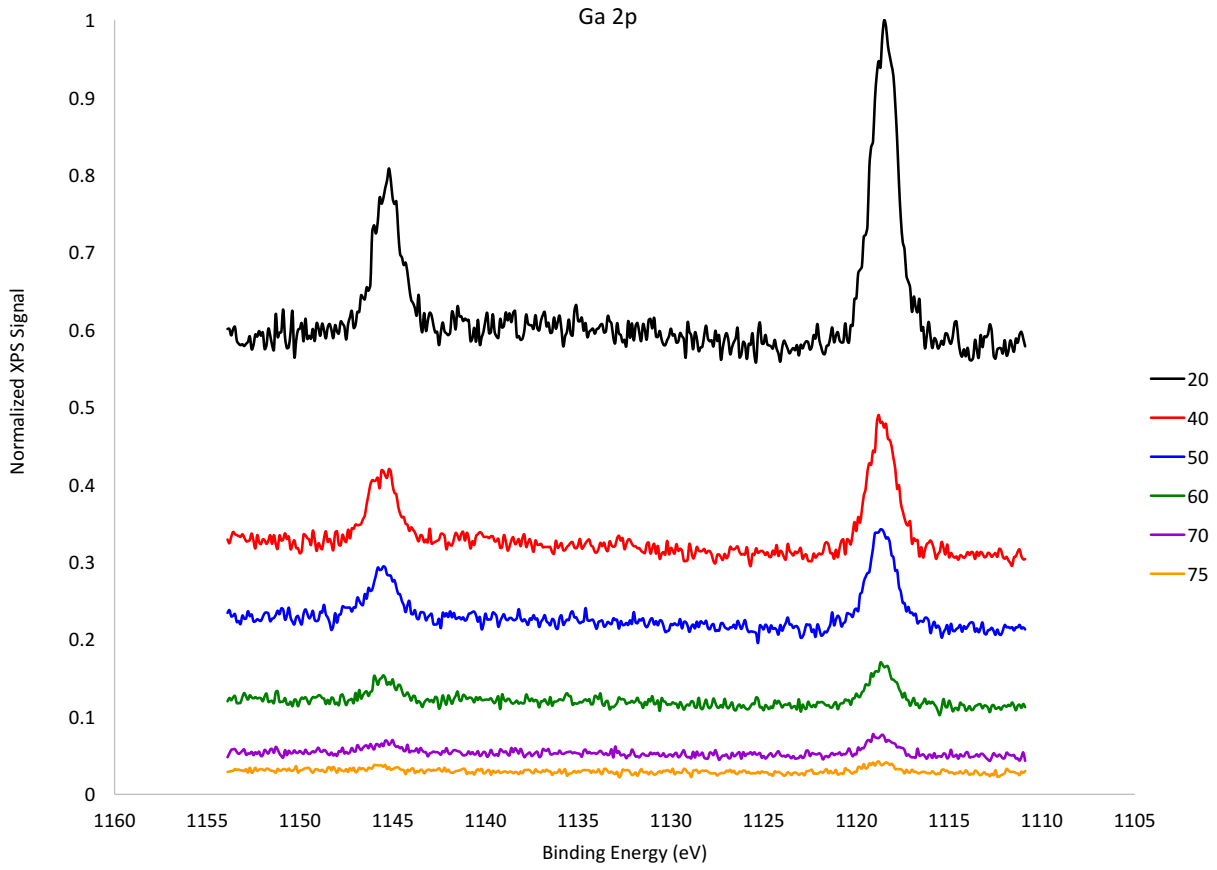

Figure S2: Gallium 2p angle resolved XPS spectra, after electroduction as described.

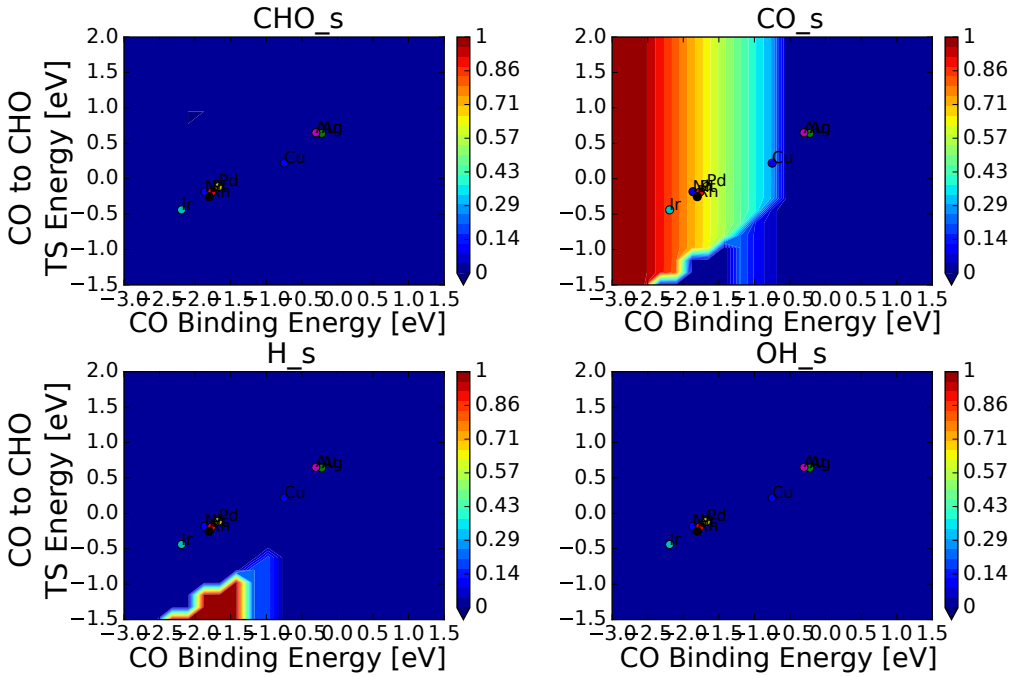

Figure S3: Surface coverages of the considered species with appreciable coverages (*H, *CO, *CHO, *OH) based on the (211) metal scaling relations and microkinetic model, as a function of the CO binding energy and the *CO→*CHO transition state energies.

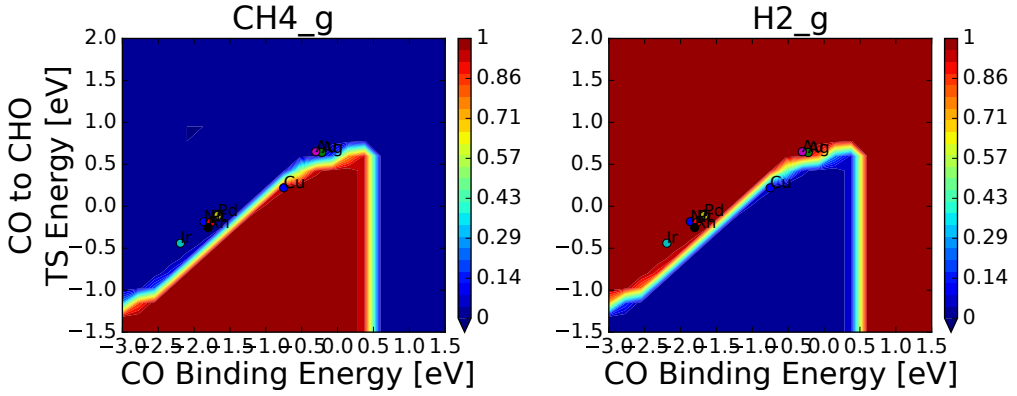

Figure S4: Selectivity towards either CH_4 or H_2 based on the (211) metal scaling relations and microkinetic model, as a function of the CO binding energy and the *CO→*CHO transition state energies